


# ANYpulator: Design and Control of a Safe Robotic Arm

**Conference Paper****Author(s):**

Bodie, Karen; Bellicoso, C. Dario; [Hutter, Marco](#) 

**Publication date:**

2016

**Permanent link:**

<https://doi.org/10.3929/ethz-a-010689402>

**Rights / license:**

[In Copyright - Non-Commercial Use Permitted](#)

**Originally published in:**

<https://doi.org/10.1109/IROS.2016.7759189>

# ANYpulator: Design and Control of a Safe Robotic Arm

Karen Bodie, C. Dario Bellicoso, and Marco Hutter

**Abstract**—The present paper introduces a manipulator that is developed to combine safe and dynamic interaction tasks. The system is built from lightweight carbon fiber links and novel high-performance series elastic actuator units that provide dynamic movement capability, low-impedance joint torque control, and inherent interaction safety. This enabled the implementation of a model-based direct force control method purely based on joint torque regulation. Using unified force and motion control, the end-effector position can be accurately and dynamically tracked in task space while acting safely upon (unexpected) contacts with the environment. The force control component is implemented in a novel way that shows reduced forces in comparison to existing methods when navigating across a surface of unpredictable orientation and friction. ANYpulator is tested using a haptic feedback method that renders the system dynamics and contact forces back to the user.

## I. INTRODUCTION

Manipulator robots have traditionally been confined to deterministic industrial environments to perform tasks in the absence of humans. The main hurdle that restricts physical collaboration between robots and humans is the requirement for safe interaction, since for most realistic scenarios a good model of the environment is not available. Safe interaction can be achieved by lowering the effective end-effector inertia and hence impact loads, while monitoring and controlling the force that a robot exerts on its environment.

### A. Safety

To be considered safe, a robot that interacts with humans must be able to act without injuring any human in its environment in regular operation or during failure, and without causing damage to itself. Human injury is based on accelerations of the contacted body part [1], which are a function of the robot's inertia, speed at impact, and contact area. To achieve speeds necessary for efficient task performance while guaranteeing a safe environment for human interaction, a low inertia manipulator is required. This demands lightweight linkages and careful mass distribution in the mechanical design. Further reduction of the effective inertia can be achieved by decoupling the motor and gear from the output load, so that link inertia is the only effective inertia seen during high speed contact. A promising way to realize this is decoupling using passive compliance as in series elastic actuation [2]. Combined with lightweight structures, series elastic joints allow for inherently safe behavior during unexpected collisions.

This work was supported in part by the the Swiss National Science Foundation through the NCCR Digital Fabrication.

All authors are with the Robotic Systems Lab, ETH Zurich, karen.bodie@mavt.ethz.ch



Fig. 1. Geomagic Touch is used for haptic teleoperation of ANYpulator

### B. State of the Art

In light of the recent push towards human-robot collaboration, a suite of force controllable robots has emerged.

The iiwa [3] developed by Kuka, and Jaco<sup>2</sup> [4] developed by Kinova are some of the most prevalent manipulator arms in robotic research with integrated torque sensors at each joint. The Jaco has an exceptionally lightweight design, with a payload-to-weight ratio of 0.59 in its 6 degree of freedom realization. While providing the ability of regulating the joint torque or contact force, all these manipulators feature traditional high-gear actuation which results in large reflected inertia at the end-effector. A different direction was taken by Rethink Robotics. Their newest robot Sawyer, a 7 degree of freedom manipulator [5], features passive compliance through series elastic actuation. While such actuation approach is criticized as having to compromise position accuracy for inherent safety [6], Sawyer contradicts this by achieving a position repeatability of 0.1 mm. This value is comparable with the actively compliant Kuka iiwa.

### C. Contribution

The contributions presented in this paper are threefold. First, we develop a safe robotic arm with highly dynamic capabilities and fast response. In this design, lightweight linkages combined with passive compliance in the form of innovative series elastic actuator modules ensure low inertia during collisions. Second, we present a novel implementation

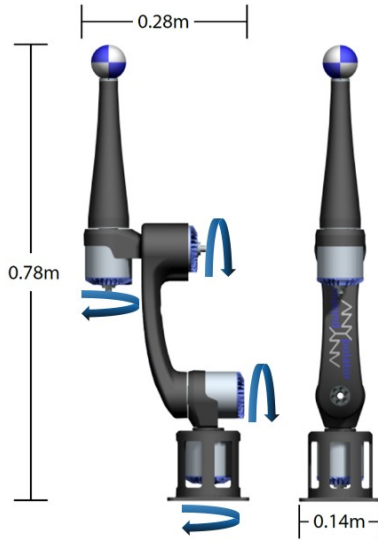


Fig. 2. ANYpulator, a compliant robotic manipulator arm.

of unified force and motion control that depends only on joint torque measurements to minimize forces on a contact surface, independent of surface friction and actual contact plane orientation. Third, we demonstrate the functionality of ANYpulator by teleoperation with dynamics-based haptic feedback that renders meaningful dynamic forces to the user, creating an intuitive sense of the environment.

## II. DESIGN

ANYpulator is a 4 degree of freedom manipulator arm composed of rigid but lightweight links paired with modular joint units with integrated passively compliant actuation (see section III). Since the joint units contain all electronics and sensors, no further transmission, bearing or sensing is integrated in the arm. The morphology was chosen anthropomorphic as an ideal solution for performing tasks in a human-oriented environment [7]. For the shorter links and base structure, precisely machined aluminum parts were manufactured. Longer links are composed of carbon fiber with aluminum interfaces, to produce lightweight rigid structures of greater length.

TABLE I  
PROPERTIES OF ANYPULATOR

Reachable sphere [m]	∅ 1.1
Range of motion	(∞, 220°, ∞, ∞)
Mass [kg]	4.8
Payload [kg]	5.0
Dimensions [m]	0.28 x 0.78 x 0.14
Torque per joint [Nm]	40
Joint speed [rad/s]	12

The current design with a spherical end-effector is extensible for additional degrees of freedom including a gripper in future applications.

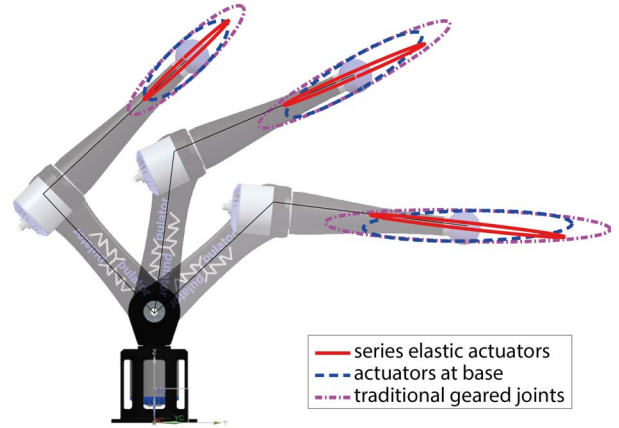


Fig. 3. Generalized inertia ellipsoids in various joint configurations for different actuation approaches

### A. Compliant Actuators for Enhanced Safety

The energy and impulse in a inelastic collision of a manipulator with the environment are

$$\Delta E = \frac{1}{2} \dot{\mathbf{x}}_E \Lambda_E \dot{\mathbf{x}}_E, \quad (1)$$

$$\Delta p = \|\Lambda_E \dot{\mathbf{x}}_E\|_2. \quad (2)$$

Both are dependent on the end-effector velocity  $\dot{\mathbf{x}}_E$  as well as the corresponding inertia

$$\Lambda_E = (\mathbf{J}_E \mathbf{M}^{-1} \mathbf{J}_E^T)^{-1}, \quad (3)$$

which is a function of the mass matrix  $\mathbf{M}$  and the end-effector Jacobian  $\mathbf{J}_E$ . For simplicity, when considering the arm as planar system, the mass matrix is given by

$$\mathbf{M} = \sum_{l \in \text{links}} (\mathbf{J}_{l,p}^T \mathbf{J}_{l,p} m_l + \mathbf{J}_{l,R}^T \mathbf{J}_{l,R} \theta_l) + \sum_{m \in \text{motors}} (\mathbf{J}_{m,p}^T \mathbf{J}_{m,p} m_m + \mathbf{J}_{m,R}^T \mathbf{J}_{m,R} \theta_m), \quad (4)$$

with the individual mass and inertia of the links ( $m_l$ ,  $\theta_l$ ) and motor ( $m_m$ ,  $\theta_m$ ). It is important to understand that the actuator inertia of a geared system with reduction  $\eta$  is largely dominated by the reflected inertia:

$$\theta_m = \theta_{\text{gearbox output}} + \eta^2 \theta_{\text{motor shaft}} \approx \eta^2 \theta_{\text{motor shaft}}. \quad (5)$$

If a manipulator should be safe and dynamic at the same time, it is necessary to lower the inertia as much as possible. While reduction of the mass matrix by improving the links is limited by material and fabrication processes, significant improvement is possible with the type and arrangement of actuation.

1) *Reducing Link Mass:* A common method (used for example in Barret's WAM arm [8]) is to reduce the mass contribution of the motors by moving all actuators to the base and introducing cable or other transmission systems:

$$\sum_{m \in \text{motors}} \mathbf{J}_{m,p}^T \mathbf{J}_{m,p} m_m = 0 \quad (6)$$

Unfortunately, this often limits the performance and position accuracy of the system and increases complexity in the design.

2) *Removing Reflected Inertia*: A second method is to reduce the inertia contribution of the motors by decoupling the motor and gear from the output using compliant elements. If this decoupling is "perfect", the actuator inertia is reduced to

$$\sum_{m \in \text{motors}} \mathbf{J}_{m,R}^T \mathbf{J}_{m,R} \theta_m = 0. \quad (7)$$

A commonly used method for decoupling is the integration of series elastic actuators.

3) *Comparison of Effectiveness*: To compare the effectiveness of moving actuators to the base against using series elastic actuators in the joints, we analyzed our manipulator using a modified analysis as initially proposed in [9]. Figure 3 displays the inertia ellipsoids of the end-effector, whereby the principal axes are determined by an Eigenvalue analysis of  $\Lambda_E$ . The ellipsoid of the traditional setup with geared motors in the joints is depicted as violet-dotted, of the setup with the actuators moved to the base ( $m_m = 0$ ) in blue dashed, and of the arm driven by series elastic actuators at the joints ( $\theta_m = 0$ ) in red solid. With a gear reduction of 1:50 as used in our actuators, the reflected inertia of the motor is about equal to having the complete motor mass in the joint, namely  $0.05 \text{ kgm}^2$ , and about 5 times larger than the inertia of the large carbon link. As a result, the Eigenvalues (and hence energy and impact) aligned with the last link are about equal in either case, while inertia perpendicular to this is significantly lower in case of a series elastic actuator. Note that this comparison does not include the additional weight due to transmission and bearing that are required for a system with remote actuators.

### B. System Comparison

The resulting specifications of ANYpulator compared with other state of the art torque controlled manipulators are shown in table II. A payload to mass ratio close to 1 is achieved, with the mass and reach comparable to the 4DOF version of Jaco<sup>2</sup> arm by Kinova.

However, ANYpulator has a maximum joint speed of about  $12 \text{ rad/s}$ , which provides peak linear velocities of  $5 \text{ m/s}$  which is significantly higher than the other manipulators (c.f. Jaco2 has  $20 \text{ cm/s}$  linear end-effector velocity [4])

TABLE II  
COMPARISON OF ANYPULATOR TO OTHER MANIPULATORS

	ANYpulator	Sawyer	Jaco2	iiwa 7
DoF	4	7	4	7
Compliance	passive	passive	active	active
Mass [kg]	4.8	19	3.6	23.9
Payload [kg]	5	4	3.5/4.4	7
Payload to Mass Ratio	1.04	0.21	0.97	0.29
Reach [m]	0.55	1.2	0.75	0.8

## III. ANYDRIVE - SAFE JOINT UNITS

The actuators of ANYpulator are designed as modular units composed of brushless high-torque motors, harmonic drive gears and a torsional spring. Absolute encoders with

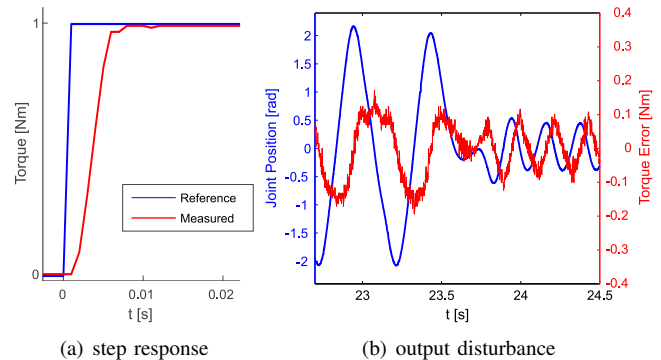


Fig. 4. The ANYdrive joint units show fast joint torque tracking (a) and good output disturbance rejection (b).

17 bit resolution measure the output position as well as the spring deflection, which can be directly related to the joint torque. This provides joint position sensing accuracy of  $0.025^\circ$  and torque resolution better than  $0.1 \text{ Nm}$ . Thanks to integrated motor control electronics, these joint modules can be simply connected over CAN and DC power bus.

### A. Joint Torque Control Structure

The joint torque control structure was adapted from the series elastic actuators employed in NASA's Valkyrie robot [10]. That is, the motor is considered a torque source controlled by a low-level Field Oriented Current (FOC) controller. The joint torque control loop is realized as simple PID controller with feed forward compensation as a function of the motor constant and gear reduction. To compensate for velocity-dependent friction, Coulomb and viscous friction were identified from several measurement samples. For small joint torque amplitudes, the proposed actuation system achieves a bandwidth as high as  $70 \text{ Hz}$ , which is reduced at high amplitudes due to motor saturation effects (e.g.  $24 \text{ Hz}$  for  $10 \text{ Nm}$ ). With this output torque controller, the system achieves a fast step response (Fig. 4(a)) and good torque tracking even in the presence of disturbance at the output (Fig. 4(b)). If the link is randomly disturbed by quick output motion (blue), the joint torque can maintain high accuracy with a maximum error of less than  $0.2 \text{ Nm}$  (red).

### B. Actuator Safety

As outlined in Sec. II-A, a very low inertia at the output can be achieved if the actuator is "perfectly" decoupled from the joint. In this context, perfect decoupling can be understood to mean that any self-imposed collision with a passive object (that may be infinitely heavy and stiff) does not lead to high loads transferred from the motor and gearbox to the output. For a series elastic actuator this means that the spring stiffness must be selected to be as low as possible and the motor dynamics as high as possible to minimize the effective joint impedance.

To validate such behavior experimentally, the actuator is commanded to produce zero torque while the output is moved at high speeds, then brought to an instantaneous rest in plastic collision. As illustrated in Fig. 5, in a very

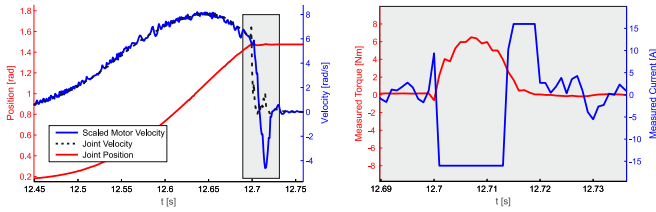


Fig. 5. Behavior of a joint actuator during perfectly plastic collision at high joint (and motor) speed

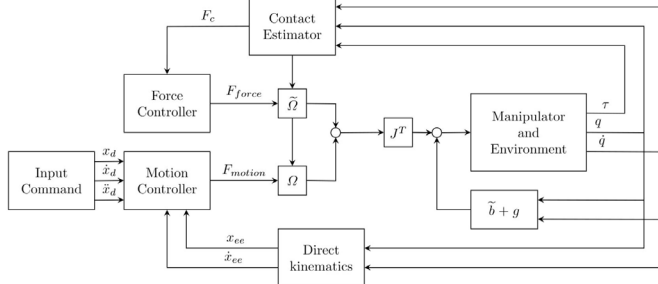


Fig. 6. Unified Motion and Force Control schematic

short time after collision with the environment, the motor is fully decelerated and brought to rest. It takes about 7 ms to stop the motor, with the joint torque remaining below 7 Nm throughout, and about 15-20 ms to reduce the joint torque to zero. With a maximum lever arm from the actuator to the contact point of 0.25 m, the resulting force applied by the actuator during collision is less than 28 N.

#### IV. CONTROL

##### A. System Model

The joint space dynamic model of the ANYpulator system can be written as

$$\boldsymbol{\tau} = \mathbf{M}(\mathbf{q})\ddot{\mathbf{q}} + \mathbf{b}(\mathbf{q}, \dot{\mathbf{q}}) + \mathbf{g}(\mathbf{q}) + \mathbf{J}_E(\mathbf{q})^T \mathbf{F}_c, \quad (8)$$

as a function of joint positions  $\mathbf{q}$ , velocities  $\dot{\mathbf{q}}$ , and accelerations  $\ddot{\mathbf{q}}$ . The torque  $\boldsymbol{\tau}$  represents the actuator torque.  $\mathbf{M}(\mathbf{q})\ddot{\mathbf{q}}$  are the inertial components,  $\mathbf{b}(\mathbf{q}, \dot{\mathbf{q}})$  incorporates Coriolis and centrifugal effects, and  $\mathbf{g}(\mathbf{q})$  represents gravitational components. The final term,  $\mathbf{J}_E(\mathbf{q})^T \mathbf{F}_c$ , represents the influence of external forces  $\mathbf{F}_c$  acting on the end-effector projected to joint space through the Jacobian transposed  $\mathbf{J}_E(\mathbf{q})^T$ . In this implementation, we are only considering forces that occur at the end-effector.

##### B. Unified Force and Motion Control

Torque feedback from the joints is required to directly control interaction forces of the manipulator. As early as 1987, Khatib [11] introduced unified motion and force control as a method of direct force control in unknown environments. In this unified approach, task specification matrices decouple the desired directions of motion and force control in operational space. In the direction of contact, the manipulator can exert a low force on an object, while maintaining free motion in the orthogonal plane. This allows

for navigation to the target position while interacting safely with the environment in contact.

Assuming that collisions involve a single point of contact, a coordinate frame is chosen such that the z-axis aligns with the direction of contact force, and the other axes lie arbitrarily in the orthogonal plane. With this we define a specification matrix,  $\boldsymbol{\Sigma}_f$ , dependent on the state of contact of the end-effector. This diagonal matrix corresponds to the directions of unconstrained motion in task space. With no detected contact, the matrix is an identity, implying free motion in all cartesian directions. If a contact is detected, the third diagonal value  $\sigma$  is set to zero, corresponding to the direction in which motion is constrained:

$$\boldsymbol{\Sigma}_f = \begin{pmatrix} 1 & 0 & 0 \\ 0 & 1 & 0 \\ 0 & 0 & \sigma \end{pmatrix} \quad \sigma = \begin{cases} 1 & \text{no contact} \\ 0 & \text{in contact} \end{cases} \quad (9)$$

Let  $\mathbf{R}$  be a rotation transformation matrix that maps between the contact force frame and the world frame. To decouple the task space, we define a selection matrix,  $\boldsymbol{\Omega}$ . When in contact, the selection matrix filters out any force prescribed in the direction of the contact force. A complimentary selection matrix  $\tilde{\boldsymbol{\Omega}}$ , selects only components in the contact force direction.

$$\boldsymbol{\Omega} = \mathbf{R}^T \boldsymbol{\Sigma}_f \mathbf{R}, \quad \tilde{\boldsymbol{\Omega}} = \mathbf{R}^T (\mathbf{I} - \boldsymbol{\Sigma}_f) \mathbf{R}. \quad (10)$$

Using  $\boldsymbol{\Lambda}_E$  as defined in (3), the vector  $\mathbf{b}$  containing centrifugal and Coriolis terms is augmented to:

$$\tilde{\mathbf{b}} = \mathbf{b} - \mathbf{J}_E^T \boldsymbol{\Lambda}_E \dot{\mathbf{J}}_E \dot{\mathbf{q}} \quad (11)$$

Motion and force commands are computed separately, and filtered using selection matrices. The motion command term  $\mathbf{F}_m^*$  is simply a task space inverse dynamics controller, while the force command term  $\mathbf{F}_f^*$  represents a limiting contact force:

$$\mathbf{F}_m^* = \ddot{\mathbf{x}}_d + \mathbf{K}_p(\mathbf{x}_d - \mathbf{x}_E) + \mathbf{K}_d(\dot{\mathbf{x}}_d - \dot{\mathbf{x}}_E) \quad (12)$$

$$\mathbf{F}_{motion} = \boldsymbol{\Omega} \boldsymbol{\Lambda}_E \mathbf{F}_m^* \quad (13)$$

$$\mathbf{F}_{force} = \tilde{\boldsymbol{\Omega}} \mathbf{F}_f^* \quad (14)$$

where desired values  $\mathbf{x}_d$ ,  $\dot{\mathbf{x}}_d$ , and  $\ddot{\mathbf{x}}_d$  are received from a tele-operating device or a path planner. Unifying these two components and feeding them back into the equations of motion produces a motor torque command

$$\tilde{\mathbf{u}} = \mathbf{J}_E^T (\mathbf{F}_{motion} + \mathbf{F}_{force}) + \tilde{\mathbf{b}} + \mathbf{g}. \quad (15)$$

Note that the dynamic equation parameters are estimates of their true values. For ease of reading, additional notation is omitted in this paper.

A simplified version of the block diagram for unified force and motion control is shown in Fig. 6. Input commands and the estimated end-effector state are processed by the motion controller, the output of which is filtered by  $\boldsymbol{\Omega}$ . Measured contact forces are processed by the force controller, then filtered by  $\tilde{\boldsymbol{\Omega}}$ . These selection matrices are generated with information from the contact force estimator. The force



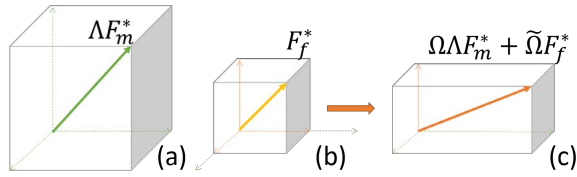


Fig. 7. Force limiting in contact with a horizontal plane showing (a) motion component, (b) limited force component (c) unified force and motion

command components are then combined, transformed to joint space, and fed through the dynamic model to send torque commands to the actuators.

### C. Force Limiting in Contact

To ensure a smooth transition between motion and contact, the desired force  $\mathbf{F}_f^*$  is constructed as:

$$\mathbf{F}_f^* = \begin{cases} \mathbf{\Lambda}_E \mathbf{F}_m^* & \text{if } \|\mathbf{\Lambda}_E \mathbf{F}_m^*\| < F_{d,max} \\ \frac{F_{d,max}}{\|\mathbf{\Lambda}_E \mathbf{F}_m^*\|} \mathbf{\Lambda}_E \mathbf{F}_m^* & \text{otherwise} \end{cases} \quad (16)$$

If the Euclidean norm of the motion control force  $\mathbf{\Lambda}_E \mathbf{F}_m^*$  is below a specified maximum desired force  $F_{d,max}$ , then the force in the contact direction is the same as that computed by motion control. When the motion control force saturates at  $F_{d,max}$ , however, force in the contact direction is capped at this limit. Figure 7 gives a geometrical visualization of this force limiting mechanism.

In reality, when estimating contact forces based on joint torque measurements, the resulting vector is a combination of normal forces and orthogonal friction forces due to contact on the plane. Unified force and motion control defines the contact force selection matrix as aligning with the direction of the contact plane, but determining this direction requires the more complex task of estimating surface contact friction.

The method proposed in this paper does not require estimating the contact plane, and instead will always keep the force in the true contact direction (including a friction component) below the desired maximum  $F_{d,max}$ . In the case where the perceived contact force vector and surface normal align, the force into the plane can reach  $F_{d,max}$ . An added benefit of this method is that when the target point traverses the contact plane, normal force is reduced relative to the desired value, thereby reducing friction and allowing smoother motion across the contact surface.

### D. Preventing Stick-Slip Effects

When testing the classical approach of limiting the force in the known contact direction, we encountered several stick-slip issues, which could also be replicated in simulation. When the arm sticks, forces in the motion plane accumulate and cause very sudden moves when overcoming the stiction force. The end-effector moves suddenly, leaves the contact surface, and is guided back by motion control, causing a jump in motion and force. This behavior could be entirely prevented by the proposed method, as it limits the buildup of friction forces in addition to forces into the contact

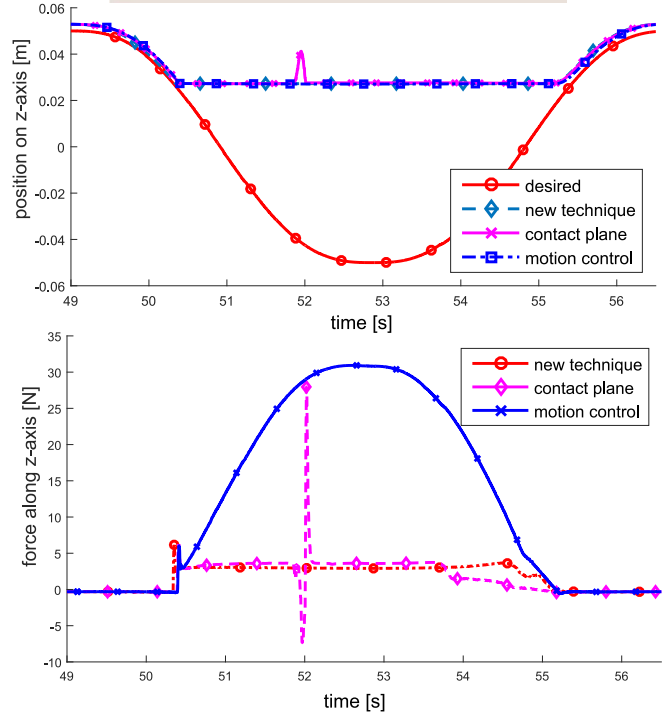
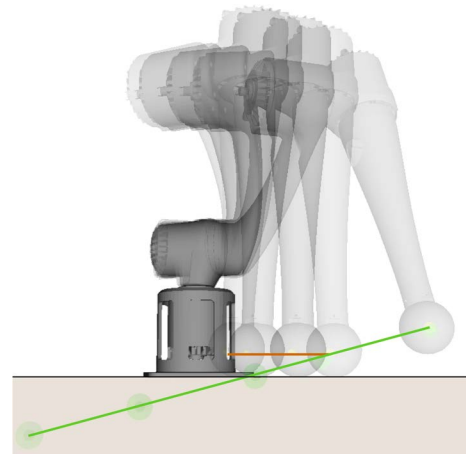


Fig. 8. Comparison of the contact behavior of different force control techniques when following a 5<sup>th</sup> order polynomial trajectory in simulation.

plane. Thereby, the total force is naturally diverted along the surface, which prevents stick-slip effects.

### E. Experimental Validation

The proposed method was implemented on ANYpulator with a desired maximum force  $F_{d,max}$  of 5 N. Figure 9 shows tracking of the end-effector force, where the desired end-effector position is being commanded by a human teleoperator to pass below the surface of a table. The estimated  $z$ -position of the end-effector, in blue, separated from tracking the desired position when it comes into contact with the table at 0.12 m. Corresponding contact forces at the end-effector in the  $z$ -direction are also shown. The cartesian norm of the estimated contact forces in  $x$ -,  $y$ - and  $z$ -directions is capped at 5 N for safe interaction with the environment.

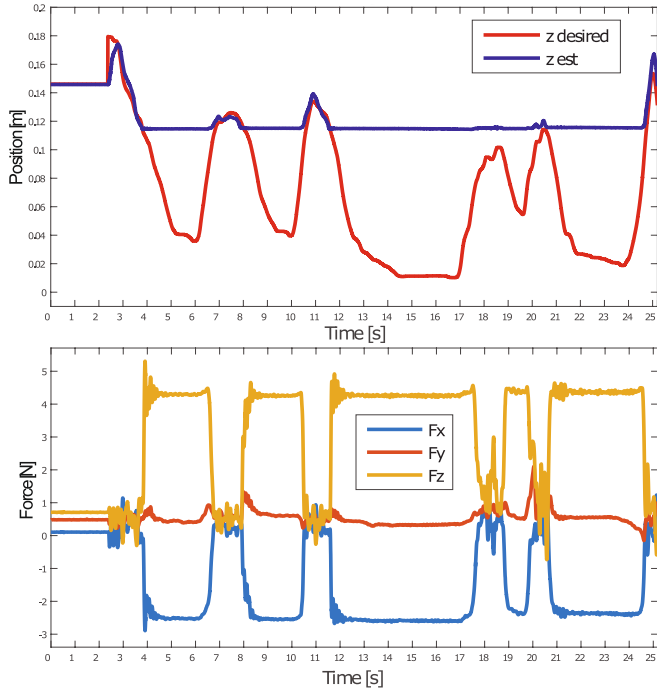


Fig. 9. Unified motion and force control in teleoperation

### F. Contact Detection

Reliable contact detection is critical for effective implementation of unified force and motion control. The series elastic actuators provide accurate joint torque measurements, from which we must deduce whether or not the robot is in contact. The present implementation is based on a generalized momentum approach, developed by de Luca et al [12][13]. Based on the conservation of momentum, the estimated error (or residual term) in the momentum equation is interpreted as a contact force. Due to modeling errors and system noise, experimentally determined thresholds on each of the residual values in joint space are used to determine if a contact has been made. For the results in this paper, only the case of contact at the end-effector is considered.

## V. HAPTIC TELEOPERATION

Haptic teleoperation has been used in a variety of applications including personal service robots [14], robotic telesurgery [15], industrial assembly [16], virtual haptic mentoring [17], and remote manipulation in dangerous environments [18]. However, very few of the existing solutions work on systems with direct force control and to the best of our knowledge, very dynamic tasks have not been tackled so far.

### A. General Implementation

Teleoperation is performed by moving the end-effector of the haptic device in space. The center of the end-effector position corresponds to the pivot point on the haptic device pen, as seen in Fig. 10(a) where the haptic force originates. To send target commands to the manipulator, a button on the

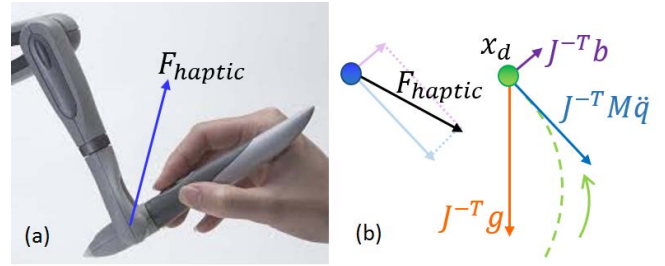


Fig. 10. (a) Haptic force (b) Dynamics-based feedback

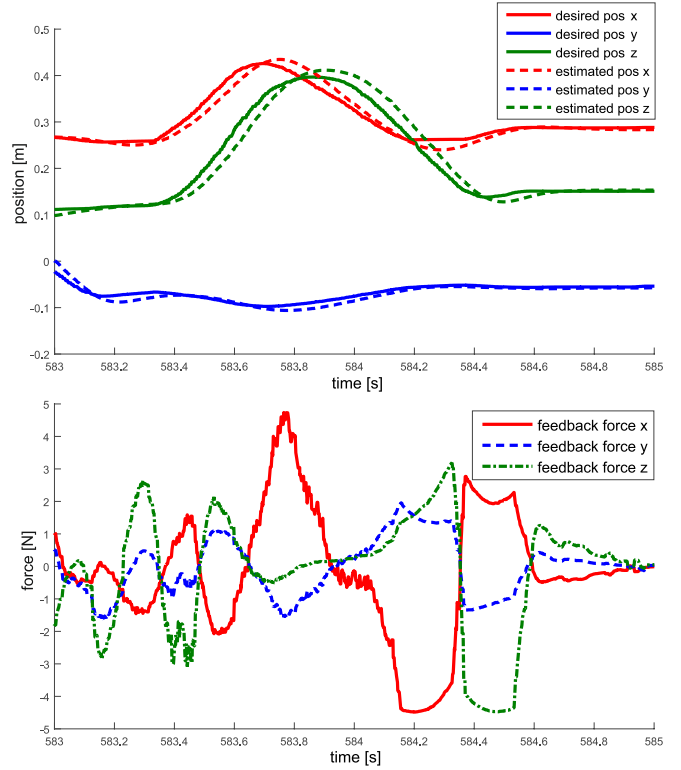


Fig. 11. (above) Position tracking and (below) corresponding feedback forces

haptic device must be pressed while the haptic pen is moved about in space. This acts as an enabling device for control, reducing the likelihood of unintentional commands and can be used to prevent the issue of different workspaces of the robot and the haptic device [19].

### B. Dynamics-Based Feedback

The motivation for dynamics-based feedback stems from a desire to provide the richest possible environmental information, namely that which we are already physically attuned to interpreting. With the physical movement of a human arm through the air, we feel the inertia of our motion, the centrifugal and Coriolis forces, and to some extent, the gravity. When the medium changes, or the payload that our hand carries changes, so do the resulting dynamics, and our sensation of the environment. In this sense, a dynamics-based feedback contains rich and useful information of the environment. An appropriate scaling factor,  $s_f$ , maximum

feedback force, and gravity compensation are applied to mitigate operator fatigue. The resulting haptic force is then

$$\mathbf{F}_{haptic} = s_f \mathbf{J}_E^{-T} (\boldsymbol{\tau} - \mathbf{g}) = s_f \mathbf{J}_E^{-T} (\mathbf{M}\ddot{\mathbf{q}} + \mathbf{b}), \quad (17)$$

with the individual components illustrated in Fig. 10(b).

Figure 11 shows the dynamics-based feedback for a position tracking operation in free space. It can be seen here that when the end-effector changes position quickly, the feedback force resists the movement, representing the inertia of the system.

To avoid oscillations of the desired position due to hand tremors during teleoperation, the target position is smoothed with an averaging filter over 30 time steps. At a communication frequency of 400 Hz, this filter results in a delay approaching 0.075 s. This small delay is not critical, since the human operator is only responsible for carrying out the task and receiving an understanding of the environment. The quick-reaction responsibilities are taken on by the unified force and motion control of the manipulator.

## VI. CONCLUSION

The present work is an attempt to realize a highly dynamic manipulator with inherent safety for interaction with humans and the environment. By building upon fast and precisely controllable series elastic actuators, the effective inertia at the output is minimized through decoupling of the gearbox and output. We demonstrated in single joint experiments that even in the worst case of full speed plastic collision with the environment, the forces due to reflected inertia are negligible. Thereby, speeds 10 times higher than in common manipulators of similar sized are reached, which demonstrates the exceptional dynamic properties of the system. While this compliant reaction to external disturbances as well as the very reactive haptic tele-manipulation is hard to depict in figures, some illustrative sequences can be found in the attached video.

The second contribution of our work is a contact force control method that allows for interaction with the environment with limited forces. Since the presented method requires neither direct measurement of contact forces at the end-effector, nor estimation of the surface friction or and contact plane direction, it has great suitability for various morphological realizations of torque sensing joints interacting with unknown environments.

With the present work we prepared a system that will enable future research of dynamic, yet safe interaction between robots and their environment.

## REFERENCES

- [1] S. Haddadin, A. Albu-Schäffer, and G. Hirzinger, "Safety evaluation of physical human-robot interaction via crash-testing," in *Robotics: Science and Systems*, vol. 3, 2007, pp. 217–224.
- [2] G. A. Pratt and M. M. Williamson, "Series elastic actuators," in *IEEE/RSJ International Conference on Intelligent Robots and Systems (IROS)*, 1995, pp. 3137–3181. [Online]. Available: <http://ieeexplore.ieee.org/lpdocs/epic03/wrapper.htm?arnumber=525827>
- [3] *Specification LBR iiwa*, Kuka, 2015, available at [www.kuka-lbr-iiwa.com](http://www.kuka-lbr-iiwa.com), version 5.
- [4] *Jaco<sup>2</sup> 4DOF Technical Specifications*, Kinova, 2015, available at [www.kinovarobotics.com/service-robotics/products/robot-arms](http://www.kinovarobotics.com/service-robotics/products/robot-arms), version 1.0.1.
- [5] Sawyer — redefining robotics and manufacturing — rethink robotics. Rethink Robotics. [Online]. Available: <http://www.rethinkrobotics.com/sawyer-intera-3>
- [6] M. Zinn, B. Roth, O. Khatib, and J. K. Salisbury, "A new actuation approach for human friendly robot design," *The international journal of robotics research*, vol. 23, no. 4–5, pp. 379–398, 2004.
- [7] C. C. Kemp, A. Edsinger, and E. Torres-Jara, "Challenges for robot manipulation in human environments," *IEEE Robotics and Automation Magazine*, vol. 14, no. 1, p. 20, 2007.
- [8] I. Barrett Technology, "WAM Arm," 2010. [Online]. Available: <http://www.barrett.com/robot/products-arm.htm>
- [9] H. Asada, "A Geometrical Representation of Manipulator Dynamics and Its Application to Arm Design," *Journal of Dynamic Systems Measurement and Control-Transactions of the Asme*, vol. 105, no. 3, 1983.
- [10] N. Paine, J. Holley, G. Johnson, and L. Sentis, "Actuator Control for the NASA-JSC Valkyrie Humanoid Robot : A Decoupled Dynamics Approach for Torque Control of Series Elastic Robots," *Journal of Field Robotics*, 2014.
- [11] O. Khatib, "A unified approach for motion and force control of robot manipulators: The operational space formulation," *Robotics and Automation, IEEE Journal of*, vol. 3, no. 1, pp. 43–53, 1987.
- [12] A. De Luca and R. Mattone, "Sensorless robot collision detection and hybrid force/motion control," in *Robotics and Automation, 2005. ICRA 2005. Proceedings of the 2005 IEEE International Conference on*. IEEE, 2005, pp. 999–1004.
- [13] E. Magrini, F. Flacco, and A. De Luca, "Control of generalized contact motion and force in physical human-robot interaction," in *Robotics and Automation (ICRA), 2015 IEEE International Conference on*. IEEE, 2015, pp. 2298–2304.
- [14] S. Muszynski, J. Stückler, and S. Behnke, "Adjustable autonomy for mobile teleoperation of personal service robots," in *RO-MAN, 2012 IEEE*. IEEE, 2012, pp. 933–940.
- [15] K. Bark, W. McMahan, A. Remington, J. Gewirtz, A. Wedmid, D. I. Lee, and K. J. Kuchenbecker, "In vivo validation of a system for haptic feedback of tool vibrations in robotic surgery," *Surgical endoscopy*, vol. 27, no. 2, pp. 656–664, 2013.
- [16] G. Salvietti, L. Meli, G. Gioioso, M. Malvezzi, and D. Prattichizzo, "Object-based bilateral telemanipulation between dissimilar kinematic structures," in *Intelligent Robots and Systems (IROS), 2013 IEEE/RSJ International Conference on*. IEEE, 2013, pp. 5451–5456.
- [17] C. L. Teo, E. Burdet, and H. Lim, "A robotic teacher of chinese handwriting," in *Haptic Interfaces for Virtual Environment and Teleoperator Systems, 2002. HAPTICS 2002. Proceedings. 10th Symposium on*. IEEE, 2002, pp. 335–341.
- [18] M. Hernando, E. Gamba, E. Pinto, and A. Barrientos, "Collision control in teleoperation by virtual force reflection. an application to the robot system," in *Robotics and Automation, 1999. Proceedings. 1999 IEEE International Conference on*, vol. 1. IEEE, 1999, pp. 565–570.
- [19] F. Conti and O. Khatib, "Spanning large workspaces using small haptic devices," in *Eurohaptics Conference, 2005 and Symposium on Haptic Interfaces for Virtual Environment and Teleoperator Systems, 2005. World Haptics 2005. First Joint*. IEEE, 2005, pp. 183–188.